Journal of Power Sources 198 (2012) 416–422

Contents lists available at SciVerse ScienceDirect

Journal of Power Sources

journal homepage: www.elsevier.com/locate/jpowsour

Pulsed laser deposition of cobalt-doped manganese oxide thin films for supercapacitor applications

Dongfang Yang*

Industrial Materials Institute, National Research Council Canada, 800 Collip Circle, London, Ontario, Canada N6G 4X8

ARTICLE INFO

Article history:
Received 13 September 2011
Accepted 3 October 2011
Available online 8 October 2011

Keywords:
Electrochemical capacitor
Supercapacitor
Ultracapacitor
Pulsed laser deposition
Cobalt-doped manganese oxides
Thin films

ABSTRACT

Thin films of manganese oxide doped with various percentages of cobalt oxide were grown by pulsed laser deposition on silicon wafers and stainless steel substrates. The films were characterized by X-ray diffraction and field emission scanning electron microscopy in order to identify their phases and microstructures. The pseudo-capacitance behavior of the Co-doped manganese oxide films were then evaluated using electrochemical cyclic voltammetry in an aqueous electrolyte. Their specific current and capacitance determined by electrochemical measurements were compared with undoped manganese oxide films, and the results show that Co-doped amorphous MnO_x films have significantly higher specific current and capacitance than undoped amorphous MnO_x films. The 3.0% Co-doped MnO_x (i.e., $Mn_{0.970}Co_{0.030}O_x$) film had the highest specific capacitance of 99 F g^{-1} at a 5 mV s^{-1} scan rate. However, Co-doped crystalline Mn_2O_3 films did not show an improvement in specific current and capacitance compared with undoped Mn_2O_3 crystalline films. High Co doping level (20.7% doped) in the crystalline Mn_2O_3 films actually decreased both the specific current and capacitance values. These findings demonstrate that elemental doping is an effective way to improve the performance of pseudo-capacitive metal oxides.

1. Introduction

Manganese oxide is regarded as the most promising candidate material among the less expensive metal oxides for pseudo-capacitor applications [1–9]. The charge storage mechanism of manganese oxide is based on surface adsorption of electrolyte cations, as well as proton incorporation, which accompanies the oxidation/reduction of Mn ions [10–14]. Manganese oxide has several advantages, such as its low cost, low toxicity, and environmental compatibility. However, several challenges need to be addressed for manganese oxides to become practical for supercapacitor active materials, namely, (i) manganese oxides have relatively low specific capacitance compared with RuO_2 [15], (ii) the partial dissolution of MnO_2 in the electrolyte leads to a decay in capacitance during charge–discharge cycling [16–18], (iii) manganese oxides have a low surface area compared with activated carbon (approximately one order of magnitude lower) [18,19], and (iv) manganese oxides have poor electronic [20] and ionic conductivity [21,22].

Doping various elements into manganese oxides to form mixed oxides has proven to be an effective way to increase the specific capacitance, electronic and ionic conduction and cycle stability of manganese oxides. Chang et al. [23] prepared binary Mn–Co oxide electrodes using anodic deposition from a mixture of aqueous manganese acetate and cobalt acetate solutions. Their experimental results indicated that addition of an appropriate amount of Co could effectively inhibit the anodic dissolution of Mn and consequently improve the electrochemical reversibility and stability of the oxide electrode. However, they also found that high Co content significantly reduced the specific capacitance of the manganese oxide. Mixtures of $Ir_{0.3}Mn_{0.7}O_2$ (30:70 mol.%) were studied by Grupioni et al. [24]. They annealed the Ir–Mn–oxide mixture at different temperatures and then studied its crystalline structure, morphology and electrochemical properties as a function of the annealing temperature. An X-ray diffraction analysis suggested possible formation of a solid solution of IrO_2 and MnO_2 between 400 and 450 °C, and the electrochemical behavior of the Ir–Mn–oxide mixture was found to depend on the annealing temperature. Because of the contribution of Ir redox transitions in the mixed oxide, a large potential window in aqueous H_2SO_4 solutions and high electroactive area were obtained. The $Ir_{0.3}Mn_{0.7}O_2$ electrodes have been found to have a large specific capacitance of nearly 550 F g^{-1}. However, the high cost of Ir has limited the wide applications of this mixed oxide.

* Tel.: +1 519 430 7147; fax: +1 519 430 7064.
E-mail address: dongfang.yang@nrc.gc.ca

0378-7753/$ – see front matter.
doi:10.1016/j.jpowsour.2011.10.008

Binary Mn–Fe oxides with different Mn/Fe ratios were prepared by Lee et al. [25,26] using anodic deposition. The deposited oxides were studied by in situ X-ray absorption spectroscopy in a 2 M KCl solution during the charge–discharge process. Their experimental results clearly confirmed that the oxidation states of both Mn and Fe changed during the charge–discharge process, which contributes to the pseudocapacitive characteristics of the binary oxides. The optimum pseudocapacitance of the binary Mn–Fe oxide could be achieved when the amount of Fe oxide was properly controlled: the highest specific capacitance of 255 F g^{-1} was obtained with a Mn/Fe atomic ratio of 90/10 while undoped Mn oxide revealed a capacitance of only 205 F g^{-1}. Their results also indicated that the incorporated iron was present in the divalent and trivalent forms in the binary oxides and that the presence of iron caused the chemical state and surface morphology of the Mn oxide electrodes to change. A decrease in capacitance values of the mixed oxide after 1000 charge–discharge cycles was 70–85% less than in the undoped Mn oxide because of the addition of iron. Nakayama et al. [27] anodically deposited Mn–Mo mixed oxide thin films on a platinum substrate from aqueous manganese (II) solutions containing the molybdate anion (MoO_4^{2-}). Cyclic voltammetry of the Mn–Mo mixed oxide film-coated electrode in aqueous 0.5 M Na_2SO_4 solution showed pseudocapacitive behavior with higher capacitance than that of the pure Mn oxide prepared under similar conditions, which was attributed by the authors to be the result of an increase in the electrical conductivity of the film. The results of electrochemical quartz crystal microbalance and X-ray photoelectron spectroscopy demonstrated that the observed pseudocapacitive behavior of the Mn–Mo mixed oxide were due to the reversible extraction/insertion of hydrated protons to balance the charge change upon oxidation/reduction of Mn^{3+}/Mn^{4+} in the film. K. R. Prasad et al. [28] used a potentiodynamic method to deposit nanostructured and microporous nickel–manganese oxide and cobalt–manganese oxide onto stainless steel substrates and characterized the mixed binary oxides by cyclic voltammetry and charge/discharge cycling in 1 M Na_2SO_4 electrolyte. Maximum specific capacitance values of 621 and 498 F g^{-1} at a CV scan rate of 10 mV s^{-1} and 377 and 307 F g^{-1} at scan rate of 200 mV s^{-1} were obtained with nickel–manganese and cobalt–manganese mixed oxide electrodes, respectively. These values are much higher than those obtained with MnO_2 alone. Long cycle-life and excellent stability of the materials were also demonstrated by those mixed oxides.

Although a number of mixed manganese oxides have been studied, there are almost no systematic studies of the effect of doping level, microstructure, and phase on the pseudocapacitive properties of mixed manganese oxides. The fundamental aspects of redox processes in mixed oxides are also poorly understood. In this work, thin films of amorphous MnO_x and crystalline Mn_2O_3 doped with cobalt oxide at various atomic percentages were deposited using pulsed laser deposition PLD on Si(1 0 0) wafers and polished stainless steel substrates and were evaluated by electrochemical CV to determine their specific current and capacitance. This paper presents a comparison of the pseudo-capacitance of Co-doped and undoped manganese oxides of different phases. The unique advantages of the PLD process for preparing supercapacitor materials, including the ease of controlling phases and microstructures and the ease of obtaining the desired stoichiometry, are also presented.

2. Experimental

2.1. Pulsed laser deposition (PLD) of manganese oxide thin films

Undoped and cobalt-doped manganese oxide films were grown on silicon and stainless steel substrates using the PLD technique.

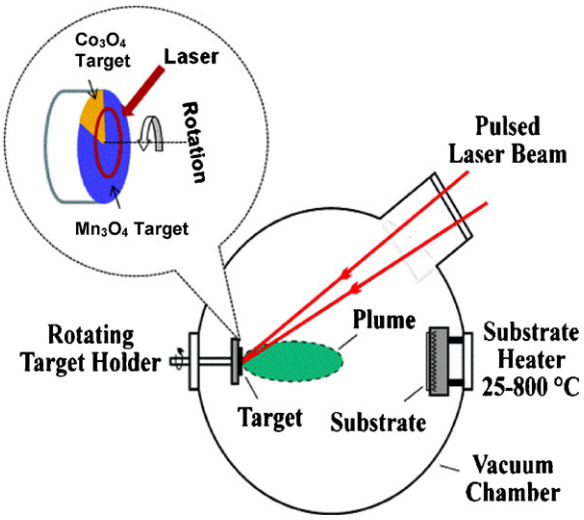

Fig. 1. Pulsed laser deposition system used for preparing the undoped and Co-doped manganese films.

The PLD process uses a pulsed laser beam generated by a KrF excimer laser (Lambda Physik LPX-210i) operating at a wavelength of 248 nm with a pulse duration of 25 ns. During deposition, the laser beam was introduced into a deposition vacuum chamber (PVD products, PLD-3000) through a quartz window and focused with an optical lens onto a target surface to ablate the target and deposit thin films in the vacuum chamber. The laser fluence on the target was adjusted to 2–3 J cm^{-2}, and the repetition rate was fixed at 50 Hz. The target used for deposition of the cobalt-doped MnO_x films consisted of a pie-shaped Co_3O_4 target at different angles mounted on top of a 3.5-in. circular Mn_3O_4 target disk (99.9% pure, from K.J. Lesker). The pie-shaped Co_3O_4 pieces were prepared by cutting a circular Co_3O_4 disk (99.9% pure, from K.J. Lesker) into various angles. The Co_3O_4/Mn_3O_4 hybrid target was subsequently ablated by the laser beam at various temperatures and oxygen pressures at a rotation speed of 18 rpm to form composite thin films deposited directly on the 3-in. Si(1 0 0) [p-type, ρ = 10–30 Ω cm, from Polishing Corporation of America] or 20 mm × 30 mm × 1.0 mm polished rectangular stainless steel 316 substrate. To improve the film homogeneities, the substrates were rotated along the vertical axis at a speed of 35 rpm. Before introducing a Si wafer into the deposition chamber, it was cleaned with acetone and isopropyl alcohol and then etched with 2.5% HF for 5 min to remove the native oxide. The stainless steel substrates were polished to a mirror-like finish using SiC sand paper and then 0.05 μm Al_2O_3 paste. The substrates were then cleaned with acetone and isopropyl alcohol before being introduced into the deposition chamber. After loading the substrates, the system was pumped down to a base pressure below 3×10^{-7} Torr using a turbo-molecular pump. Each substrate to be coated faced the target, at a stand-off distance of 8–12 cm. During deposition, the substrates were heated, under vacuum, using a programmable non-contact radioactive heater. The oxygen gas pressure was adjusted to 100 mTorr during deposition. A schematic diagram of the PLD system and the ablation setup for the Co_3O_4/Mn_3O_4 hybrid target used in this study are shown in Fig. 1, and detailed information about the deposition processes has been provided in a previous communication [29]. The film structure was examined using X-ray diffraction equipment (XRD, Philips, X-Pert MRD) with monochromatized Cu K_α radiation in the θ_0–2θ thin film configuration, where θ_0 was fixed at 0.5°. The surface morphology and chemical composition of the films was then analyzed using a Leo 440 field emission scanning electron microscope (FE-SEM) equipped with a Gresham light

Table 1
Atomic ratio of Mn and Co for various Co-doped MnO_x films deposited by PLD.

Atomic percentage for sample $Mn_{1-y}Co_yO_x$	$(1-y)_{Mn}$	$(y)_{Co}$
Mn–Co–O_x (200 °C, 100 mTorr, 15° Co_3O_4 pie-shaped piece)	0.970	0.030
Mn–Co–O_x (200 °C, 100 mTorr, 30° Co_3O_4 pie-shaped piece)	0.907	0.093
Mn–Co–O_x (200 °C, 100 mTorr, 45° Co_3O_4 pie-shaped piece)	0.774	0.226
Mn–Co–O_x (500 °C, 100 mTorr, 15° Co_3O_4 pie-shaped piece)	0.951	0.049
Mn–Co–O_x (500 °C, 100 mTorr, 30° Co_3O_4 pie-shaped piece)	0.928	0.072
Mn–Co–O_x (500 °C, 100 mTorr, 45° Co_3O_4 pie-shaped piece)	0.793	0.207

element detector and a Quartz XOne EDX system. The reflectance of the films in the ultra-violet (UV) and visible wavelength ranges was measured using a photospectrometer from Scientific Computing International. The thickness of films determined from the reflectance data was in the range of 100–400 nm. The weight of Co-doped MnO_x films was calculated from the difference in weight of the coated and the uncoated substrates measured with a highly sensitive balance with precision down to 10 μg.

2.2. Electrochemical characterization

A electrochemical characterization of Co-doped and undoped manganese oxide films was performed by cyclic voltammetry (CV) in a standard three-electrode cell with 0.1 M Na_2SO_4 aqueous solution as the electrolyte. Neutral to mildly basic pH aqueous electrolytes, such as K_2SO_4, KNO_3, and Li_2SO_4, at concentrations ranging from 0.1 M to 1 M are normally used for the electrochemical testing of manganese oxides [15,30–33]. Strong acidic or strong alkaline electrolytes, such as H_2SO_4 or KOH, are not used because manganese oxide films readily dissolve either in strong acidic or alkaline electrolytes at high potentials [34]. In addition, mild electrolytes can improve the safety issues typically encountered with the use of strong acids or bases. The counter electrode was a platinized platinum wire, and the reference electrode was an Ag/AgCl electrode fitted with a salt bridge. The potential was cycled with a Gamry PC3 potentiostat within a potential range of 0.1–0.9 V and Ag/AgCl at scan rates of 5, 10, 20 and 50 mV s^{-1}. This potential range was chosen to ensure that redox processes in Co-doped and undoped manganese oxide films occur homogenously and reversibly. The test cell configuration was designed such that all the thin-film samples have the same surface area (~4.6 cm^2) exposed to the electrolyte during the electrochemical cycling experiments. The uniform surface areas ensure that the capacitance of Co-doped and undoped manganese oxides can be compared. The specific current and capacitance of Co-doped and undoped manganese oxide films were calculated from cyclic voltammetry data and the weight of the films.

3. Results and discussions

3.1. FE-SEM/EDX characterization of Co-doped manganese oxide films deposited by PLD

The undoped and Co-doped manganese oxide films with varying Co content were grown on silicon substrates using the PLD technique. During the PLD process, a KrF excimer laser was used to ablate the hybrid Mn_3O_4/Co_3O_4 target, which consists of a 3.5-in. diameter pie-shaped Co_3O_4 target piece at 15°, 30° and 45° placed on top of a 3.5-in. circular Mn_3O_4 target at 200 °C or 500 °C in 100 mTorr O_2 to produce various Co-doped MnO_x films. The chemical compositions of the Co-doped composite films with varying Co contents were investigated by Energy Dispersive X-ray analysis (EDX). Fig. 2 shows a typical EDX spectrum of Co-doped manganese oxide excited by an electron beam (5 kV). Peaks for the elements O, Si, Mn, Co and C were observed, and the atomic percentage of the constituent elements was calculated from the EDX spectrum (see the insert table in Fig. 2). The Si originated from the substrate, and C is from surface contamination. The atomic ratios of Mn and Co for various Co-doped manganese oxide films deposited by PLD are listed in Table 1.

Fig. 3(a)–(d) shows the FE-SEM top surface images of manganese oxide film and various Co-doped manganese oxide films deposited by PLD at 200 °C in 100 mTorr O_2. The undoped MnO_x films exhibited a smooth and homogenous structure, consisting of very fine grains, with grain size of approximately 20 nm and no pores. Many larger particles of approximately 100 nm that consist of fine grains of similar size also emerged on the top of the smooth structure, as shown in Fig. 3(a). When 3.0% Co ions were doped into the MnO_x film, the very fine grains aggregated together to form particle clusters with sizes of approximately 70 nm, and the surface of the film became rougher. The larger particles of approximately 100 nm that existed in the pure MnO_x film also appeared on the top of the doped film, as shown in Fig. 3(b). When the Co doping level was increased further, many "needle-like" particles with lengths of 100–300 nm appeared on the top of the smooth film surface, as shown in Fig. 3(c) and (d). The number of "needle-like" particles decreased when the Co ion doping increased from 9.3% to 22.6%, but the "needle-like" particles became bigger. EDX was used to analyze the chemical composition of the "needle-like" particles, and their composition was compared with that of the smooth area of the film surface. The results showed that the "needle-like" particles had about 12% less Co than did the smooth area.

Fig. 4(a)–(d) shows the FE-SEM top surface images of the manganese oxide film and various Co-doped manganese oxide films deposited by PLD at 500 °C in 100 mTorr O_2. The pure manganese oxide deposited at high temperature exhibited a smooth and homogenous structure, consisting of very fine grains with a grain size of approximately 20 nm. No larger particles appeared on the top of the smooth structure, as shown in Fig. 4(a). However, the fine grains present in the high temperature deposited film aggregated to form many domains. The fine grains within each domain

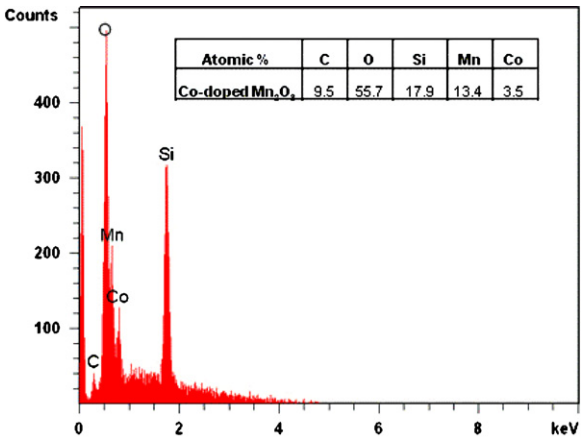

Fig. 2. EDX spectrum of the Co doped-MnO_x films deposited by PLD on Si(1 0 0) at 500 °C in 100 mTorr O_2 using a 45° pie shaped Co_3O_4 target piece mounted on the top of a circular Mn_3O_4 target.

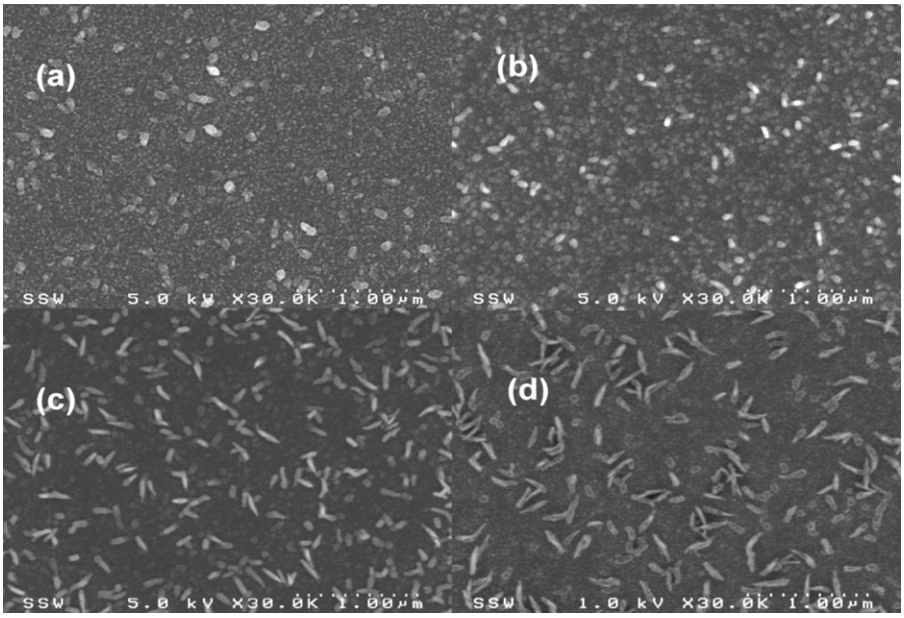

Fig. 3. FESEM images of the top surface of manganese oxide and Co-doped manganese oxide films deposited by PLD at 200 °C in 100 mTorr O_2: (a) pure MnO_x film, (b) $Mn_{0.970}Co_{0.030}O_x$ film, (c) $Mn_{0.907}Co_{0.093}O_x$ film, and (d) $Mn_{0.774}Co_{0.226}O_x$ film.

orientated in the same direction whereas fine grains in different domains oriented in different directions. When a low percentage of Co was doped into the manganese oxide film at high temperature, no "needle-like" particles appeared. The doped films had similar microstructures to the undoped films, which consisted of many domains with oriented fine grains. The size of the domains in the doped films, however, was larger than in the undoped films, and the size increased as the percentage of Co doping increased, as shown in Fig. 4(b) and (c). When Co ion substitution reached 20.7%, however, a significant change in microstructure of the film appeared. All the domains disappeared, and fine grains within the domains transformed to larger grains with a grain size of approximately 60 nm. The FE-SEM images in Figs. 3 and 4 show clearly that Co doping could significantly alter the microstructure of manganese oxide films, eventually inducing changes in their pseudo-capacitance behavior.

3.2. XRD characterization of Co-doped manganese oxide films deposited by PLD

XRD patterns of undoped and Co-doped MnO_x films of various cobalt contents, deposited on a silicon substrate at 200 °C in 100 mTorr O_2, are shown in Fig. 5. At a substrate temperature of 200 °C, all the undoped and Co-doped MnO_x films were amorphous, showing diffuse-scattering curves with very broad and poorly defined peaks centered at 2θ of about 28, 38 and 57°. This result

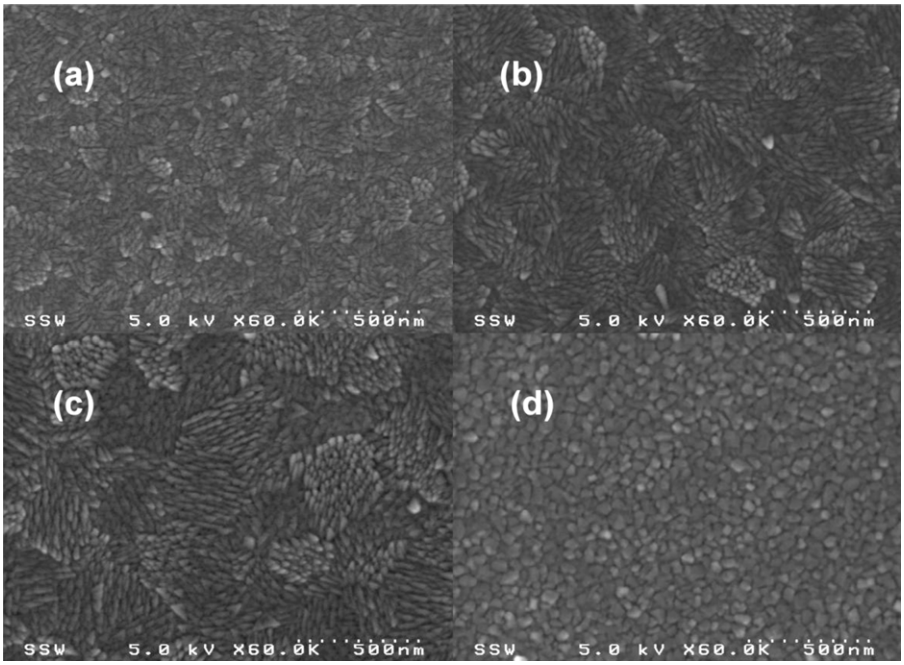

Fig. 4. FESEM images of the top surface of manganese oxide and Co-doped manganese oxide films deposited by PLD at 500 °C in 100 mTorr O_2: (a) pure Mn_2O_3 film, (b) $(Mn_{0.951}Co_{0.049})_2O_3$ film, (c) $(Mn_{0.928}Co_{0.072})_2O_3$ film, and (d) $(Mn_{0.793}Co_{0.207})_2O_3$ film.

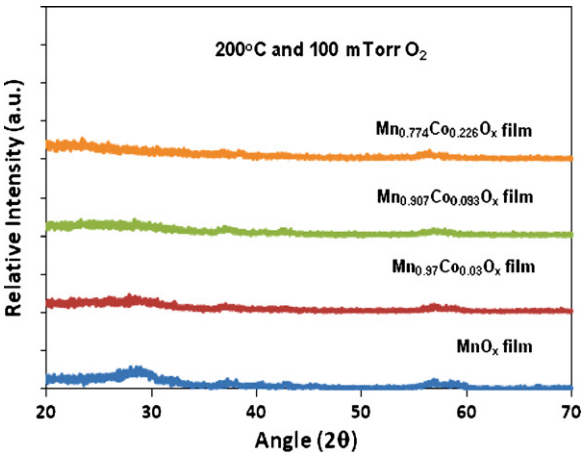

Fig. 5. XRD spectra of Co-doped manganese oxide films deposited by PLD at 200 °C in 100 mTorr oxygen gas pressure using a hybrid Mn_3O_4/Co_3O_4 target.

is consistent with the FE-SEM results presented in Fig. 3, where very fine grains of ~20 nm were the basic components present for the low temperature deposited undoped and Co-doped MnO_x films. When the deposition temperature rises to 500 °C, well-defined and sharp diffraction peaks appeared for undoped and Co-doped manganese oxide films, as shown in Fig. 6. The peak positions of the XRD spectra match to either a cubic structure (PDF card #41-1442) or an orthorhombic structure (PDF card #24-0508) of a Mn_2O_3 phase. There were no diffraction peaks originating from CoO, Co_2O_3 or Co_3O_4 present in the XRD spectra; this result indicates that Co ions are dispersed uniformly into the Mn_2O_3 lattice to form a solid solution. The features in the XRD pattern indicate that cobalt doping up to 20.7% ($(Mn_{0.793}Co_{0.207})_2O_3$, i.e., 20.7% of Mn ions substituted by Co) does not change the crystal structure of the Mn_2O_3 phase. The XRD patterns of undoped and Co-doped Mn_2O_3 films with cobalt ion doping up to 7.2% were very similar, except the peak positions shifted slightly to higher 2θ angles for the Co-doped films. However, when the Co doping increased to 20.7%, the intensity of XRD peaks decreased significantly. This result is consistent with a dramatic change in the microstructure for the 20.7% Co-doped film, as shown in FE-SEM images in Fig. 4(d). The intensity of the XRD peaks for the undoped and low Co-doped Mn_2O_3 film were greater than those observed for the 20.7% Co-doped film because in those films, domains existed in which fine grains were oriented in the same direction. The oriented fine grains in each domain all contributed

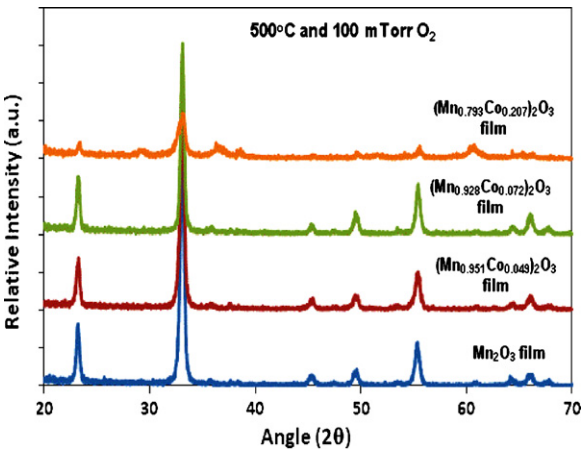

Fig. 6. XRD spectra of Co-doped manganese oxide films deposited by PLD at substrate temperatures of 500 °C in 100 mTorr oxygen gas pressure using a hybrid Mn_3O_4/Co_3O_4 target.

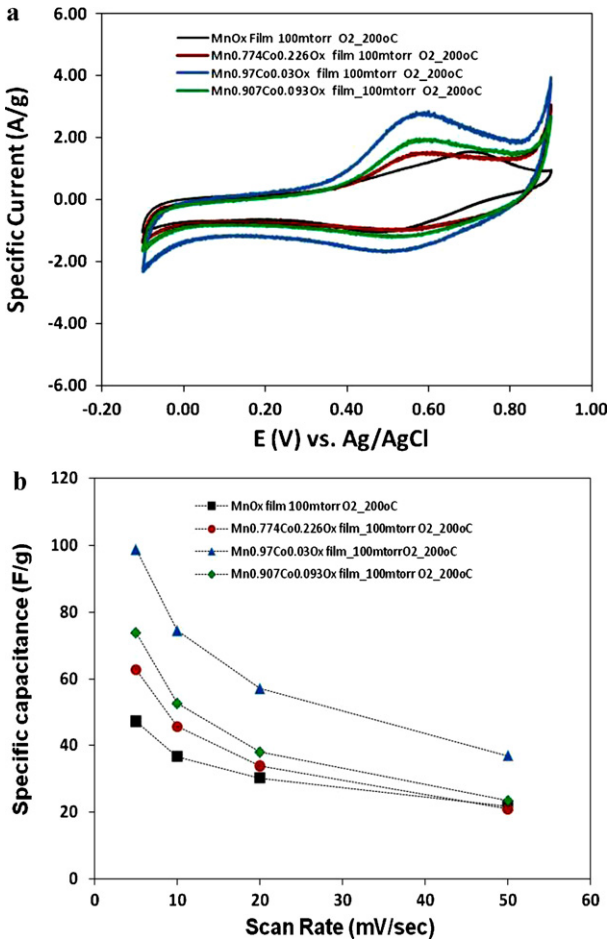

Fig. 7. Cyclic voltammetry (a) and specific capacitance (b) of amorphous MnO_x film and various Co-doped amorphous MnO_x films deposited by PLD at 200 °C in 100 mTorr of O_2.

to the XRD peak intensity at the same 2θ angle and were observed by X-ray. This observation was similar for large grains with a grain size equivalent to the domain size, although the size of the fine grains that made up the domains in undoped and low Co-doped Mn_2O_3 films were actually smaller than those of the grains in the 20.7% Co-doped film. The XRD patterns depicted in Figs. 5 and 6 clearly show that Co was dispersed uniformly into the Mn_2O_3 lattice, replacing Mn ions and not changing the phase of the structure. However, Co-doping did change the microstructure of the Mn_2O_3 films, which certainly affected their pseudo-capacitance behavior, as shown by the electrochemical measurements in the following section.

3.3. *Electrochemical characterization of cobalt-doped MnO_x films*

Electrochemical cyclic voltammetry measurements (CVs) were used to evaluate the effect of Co doping on the pseudo-capacitance behavior of manganese oxide films deposited both at 200 °C and 500 °C in 100 mTorr O_2. CVs recorded at a 20 mV s^{-1} scan rate for undoped and Co-doped amorphous MnO_x films, deposited at 200 °C by PLD, are also shown in Fig. 7(a), and their specific capacitance determined from the CV curves at scan rates of 5, 10, 20 and 50 mV s^{-1} are shown in Fig. 7(b). The CV and specific capacitance for undoped and Co-doped crystalline Mn_2O_3 films are also shown in Fig. 8(a) and (b), respectively. The CVs in Fig. 7 shows that the Co-doped amorphous MnO_x films have larger specific currents and capacitances than the undoped amorphous MnO_x film. Low cobalt doping (3.0%) had the greatest increase in capacitance,

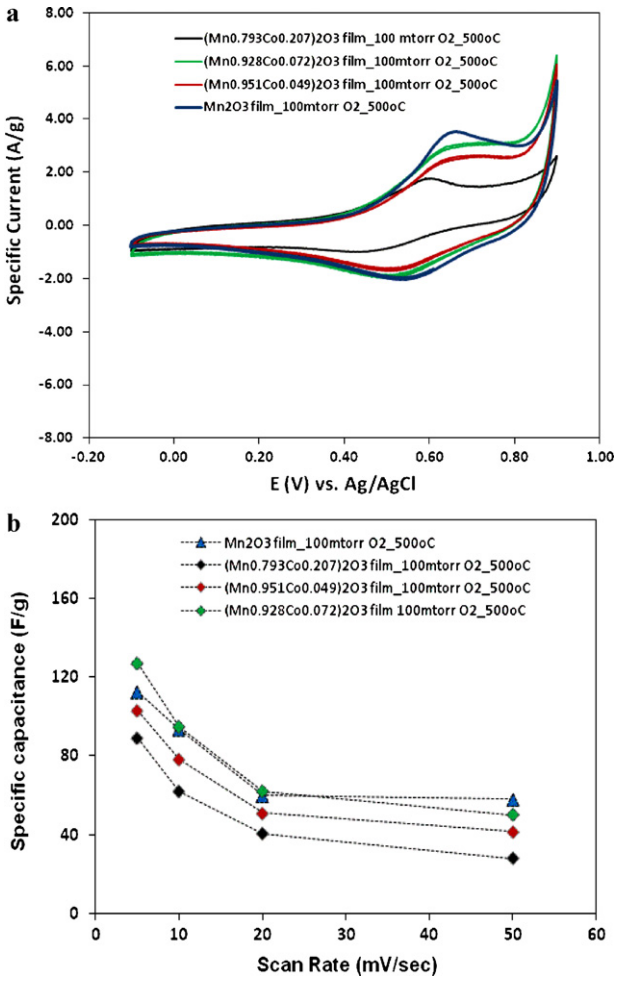

Fig. 8. Cyclic voltammetry (a) and specific capacitance (b) of a crystalline Mn_2O_3 film and various Co-doped crystalline Mn_2O_3 films deposited by PLD at 500 °C in 100 mTorr of O_2.

followed by 9.3% cobalt doping. The 22.6% cobalt doping had the least increase in specific capacitance. The operating potential window (between H_2 evolution and O_2 evolution due to decomposition of water) was shifted about 100 mV toward more negative potentials for all the Co-doped films. At a 5 mV s^{-1} scan rate, the 3.0% Co-doped MnO_x film reached 99 F g^{-1}, which is more than double that the 47 F g^{-1} observed for the undoped MnO_x film. This result indicates that Co doping significantly improves the pseudo-capacitance performance of amorphous manganese oxide. Co doping into the crystalline Mn_2O_3 film, however, did not improve the pseudo-capacitance behavior, as shown in Fig. 8. In Fig. 8(a), the CVs recorded at 20 mV s^{-1} scan rate for a 7.2% cobalt-doped Mn_2O_3 film had a similar specific current value to the undoped one, and 4.9% and 20.7% Co-doped Mn_2O_3 films had lower specific current values. The values for the 20.7% Co-doped Mn_2O_3 film were significantly lower than the undoped film. Similar trends in specific capacitance for undoped and Co-doped Mn_2O_3 films were maintained at various scan rates, as shown in Fig. 8(b).

For the amorphous MnO_x, Co-doping significantly increased its specific capacitance, showing the great benefit of mixing the two oxides. A higher specific capacitance for Co-doped manganese oxide prepared by potentiodynamic methods on stainless steel substrates was also reported by K. R. Prasad et al. [28]. The mixed oxide film deposited by the potentiodynamic method also exhibited an amorphous structure with Co substitution for Mn ions in the mixed oxide up to 23.7%. A specific capacitance value as high as 498 F g^{-1} was obtained by the authors at a CV scan rate of 10 mV s^{-1} which was attributed to the high surface area of the microporous nanostructures, as well as the high water content in the wet-electrochemically prepared mixed oxides, which increased the ionic transport. The Co-doped amorphous MnO_x films deposited by PLD in our study had specific capacitance values that were much lower than those reported by K. R. Prasad. The undoped and Co-doped manganese oxide films deposited by PLD in our study were very smooth and dense, as shown by FE-SEM images in Figs. 3 and 4. The objective of our study was to investigate the effect of Co doping and doping levels on the pseudo-capacitance performance of manganese oxides; therefore, all the undoped and Co-doped films were prepared with precise control of the chemical composition on very smooth silicon and stainless steel substrates under identical deposition processing conditions in order to achieve similar surface roughnesses and thus allow direct comparisons. The PLD processing parameters for depositing thin films in our study were not optimized (parameters such as laser energy, repetition rate, process gas pressure and temperature) to deposit large surface areas of micro/nano-porous structured films; therefore, higher specific capacitance values for the Co-doped or undoped manganese oxides were not achieved.

The FE-SEM results shown in Fig. 3 clearly indicate that even with the same deposition processing parameters, Co-doped and undoped amorphous MnO_x films possess very different surface microstructures. Surface microstructure changes induced by Co doping affect their specific capacitance values because of corresponding changes in surface area and electronic and ionic conductivity. In addition, Co doping introduces new redox couples, such as Co(II)/Co(III), Co(III)/Co(IV), which also contribute to the pseudo-capacitance behavior of the doped oxide films. A number of studies have reported the pseudo-capacitance properties of Cobalt oxide; for example, Co oxide prepared by sol–gel methods possesses a high-specific capacitance of approximately 290 F g^{-1}, as reported by Lin et al. [35], and electrodeposited Co oxide shows a capacitance of 164 F g^{-1} [36]. The major drawbacks of Co oxide compared with the Mn-based oxides for supercapacitor applications are the narrow operation potential window of approximately 0.5 V and the requirement of a basic working electrolyte, such as NaOH. Mixing cobalt oxide with manganese oxide generates a larger operational potential window than the pure Co oxide, and the mixed oxide can also work with neutral electrolytes, such as K_2SO_4. The specific capacitance for Co-doped amorphous MnO_x films observed in this study is a summary of the contributions from redox reactions of both Co and Mn oxides. The highest specific capacitance in our study was observed for the 3.0% Co-doped MnO_x film. This finding indicates that 3.0% Co doping results in an optimized electrochemical redox reaction rate, a large surface area and high electronic and/or ionic conductivity and thus an improved pseudo-capacitance. Given the available experimental results, it is difficult to identify the dominant factors that contributed to the Co-doping induced changes in pseudo-capacitance behavior.

The doping of Co into the crystalline Mn_2O_3 film did not improve in its pseudo-capacitance behavior, and a high Co doping level of 20.7% significantly reduced the specific capacitance. As shown in Fig. 4, the 20.7% Co doped Mn_2O_3 films had very different microstructures as compared with the undoped and low Co-content Mn_2O_3 films. Nevertheless, it is difficult to attribute the decrease in specific capacitance of the 20.7% Co-doped Mn_2O_3 film directly to the microstructure differences, since other factors, such as electrochemical redox reactions and film conductivity, also play important roles. To our knowledge, there is no other report on the pseudo-capacitance behavior of Co-doped, crystalline Mn_2O_3 that allows for comparison. However, J.-K. Chang et al. [23] found that a high Co content in γ-MnO_2 (with Co doping up to 18%) could also cause a significant reduction in the specific capacitance of the

manganese oxide. Moreover, E. Machefaux et al. [37] have shown that Co-doped γ-MnO_2 compounds (with Co doping of 2% and 3%) prepared by the electrochemical–hydrothermal route do not improve the specific capacitance relative to the undoped γ-MnO_2 but that Al doping does increase the specific capacitance of γ-MnO_2 because of the beneficial effect of doping on increasing the surface area of γ-MnO_2.

The significant reduction in the specific capacitance of crystalline Mn_2O_3 film by high Co doping indicates that doped Co oxide is less electroactive relative to pure Mn_2O_3 in terms of pseudocapacitance. In addition, since the capacitance of Mn_2O_3 is determined by a reversible, fast, and continuous redox reaction between its trivalent and tetravalent states, unwanted side reactions, such as $Mn_2O_3 + Co_2O_3 + 2H_2O \rightarrow 2MnO_2 + 2Co(OH)_2$ and $Mn_2O_3 + 2CoOOH + H_2O \rightarrow 2MnO_2 + 2Co(OH)_2$, that occur during the electrochemical measurement for Co-doped Mn_2O_3 films could hinder the ideal pseudocapacitive reaction and thereby decrease the overall specific capacitance of the crystalline Mn_2O_3 film [21]. To more fully understand the pseudo-capacitance behavior of mixed oxides, such as Co-doped manganese oxide, additional studies are necessary. A series of techniques such as X-ray photoelectron spectroscopy (XPS) and X-ray absorption fine structure spectroscopy (XAFS) are currently under investigation to study the structure and bonding of the Co-doped manganese oxide materials, and the results will be reported in a future communication.

4. Conclusion

Cobalt-doped amorphous MnO_x and crystalline Mn_2O_3 films have been deposited by PLD on Si(1 0 0) and stainless steel substrates in 100 mTorr O_2 pressure at temperatures of 200 °C and 500 °C. Electrochemical measurements showed that Co-doped amorphous MnO_x films have significantly higher specific current and capacitance than the undoped amorphous MnO_x films; however, Co-doped crystalline Mn_2O_3 films did not improve specific current and capacitance in comparison with the undoped crystalline Mn_2O_3 films. At a scan rate of 5 mV s^{-1}, a 3.0% Co-doped MnO_x film reached 99 F g^{-1}, which is more than double the 47 F g^{-1} observed for the undoped MnO_x film. This study demonstrates that elemental doping is an effective way to improve the performance of pseudo-capacitive metal oxides and that PLD is a suitable technique for elemental doping studies on active electrode materials for supercapacitor applications.

Acknowledgements

The author would like to thank Transport Canada and National Research Council of Canada's automotive office for supporting this supercapacitor project. The author is also indebted to Mr. B. Gibson and Mr. M. Zeman of NRC-IMI for their technical assistance. Thanks are also given to Dr. Yves Grincourt for his technical review and critical comments on this paper.

References

[1] S.E. Chun, S.I. Pyun, G.J. Lee, Electrochim. Acta 51 (28) (2006) 6479–6486.
[2] L. Li, Z.Y. Qin, L.F. Wang, H.J. Liu, M.F. Zhu, J. Nanopart. Res. 12 (2010) 2349–2353.
[3] J.K. Chang, Y.L. Chen, W.T. Tsai, J. Power Sources 135 (2004) 344–353.
[4] V. Subramanian, H. Zhu, B. Wei, Chem. Phys. Lett. 453 (2008) 242–249.
[5] M.S. Wu, P.J. Chiang, Electrochem. Commun. 8 (2006) 383–388.
[6] M. Nakayama, T. Kanaya, R. Inoue, Electrochem. Commun. 9 (2007) 1154–1158.
[7] X. Wang, Y. Li, J. Chem. Eur. 9 (2003) 300–306.
[8] C.-C. Hu, K.-H. Chang, M.-C. Lin, Y.-T. Wu, Nano Letters 6 (2006) 2690–2695.
[9] M. Jayalakshmi, K. Balasubramanian, Int. J. Electrochem. Sci. 3 (2008) 1196–1217.
[10] C.C. Hu, T.W. Tsou, Electrochem. Commun. 4 (2002) 105–109.
[11] B. Messaoudi, S. Joiret, M. Keddam, H. Takenouti, Electrochim. Acta 46 (2001) 2487–2498.
[12] S.C. Pang, M.A. Anderson, J. Mater. Res. 15 (2000) 2096–2106.
[13] E. Raymundo-Pinero, V. Khomenko, E. Frackowiak, F. Beguin, J. Electrochem. Soc. 152 (2005) A229–A235.
[14] C. Ye, Z.M. Lin, S.Z. Hui, J. Electrochem. Soc. 152 (2005) A1272–A1278.
[15] A.E. Fischer, M.P. Saunders, K.A. Pettigrew, D.R. Rolison, J.W. Long, J. Electrochem. Soc. 155 (3) (2008) A246–A252.
[16] Y.C. Hsieh, K.T. Lee, Y.P. Lin, N.L. Wu, S.W. Donne, J. Power Sources 177 (2008) 660–664.
[17] Q. Li, K. Li, J. Gu, H. Fan, J. Phys. Chem. Solids 69 (2008) 1733–1739.
[18] T. Brousse, M. Toupin, R. Dugas, L. Athouel, O. Crosnier, D. Belanger, J. Electrochem. Soc. 153 (2006) A2171–A2180.
[19] D. Qu, H. Shi, J. Power Sources 74 (1998) 99–107.
[20] B. Babakhani, D.G. Ivey, J. Power Sources 195 (2010) 2110–2117.
[21] M. Toupin, T. Brousse, D. Bélanger, Chem. Mater. 14 (2002) 3946–3952.
[22] H.Y. Lee, S.W. Kim, H.Y. Lee, Electrochem. Solid State Lett. 4 (2001) A19–A22.
[23] J.-K. Chang, M.-T. Lee, C.-H. Huang, W.-T. Tsai, Mater. Chem. Phys. 108 (1) (2008) 124–131.
[24] F. Grupioni, E. Arashiro, T.A.F. Lassali, Electrochim. Acta 48 (4) (2002) 407–418.
[25] M.-T. Lee, J.-K. Chang, W.-T. Tsai, C.-K. Lin, J. Power Sources 178 (1) (2008) 476–482.
[26] M.-T. Lee, J.-K. Chang, W.-T. Tsai, J. Electrochem. Soc. 154 (9) (2007) A875–A881.
[27] M. Nakayama, A. Tanaka, Y. Sato, T. Tonosaki, K. Ogura, Langmuir 21 (13) (2005) 5907–5913.
[28] K. Rajendra Prasad, N. Miura, Electrochem. Commun. 6 (10) (2004) 1004–1008.
[29] S. Boughaba, G.I. Sproule, J.P. McCaffrey, M. Islam, M.J. Graham, Thin Solid Films 358 (2000) 104–113.
[30] C. Xu, F. Kang, B. Li, H. Du, J. Mater. Res. 25 (8) (2010) 1421–1432.
[31] T. Brousse, P.-L. Taberna, O. Crosnier, R. Dugas, P. Guillemet, Y. Scudeller, Y. Zhoud, F. Favier, D. Bèlanger, P. Simon, J. Power Sources 173 (2007) 633–641.
[32] T. Brousse, M. Toupin, D. Bèlanger, J. Electrochem. Soc. 151 (4) (2004) A614–A622.
[33] N. Wang, H. Pang, H. Peng, G. Li, X. Chen, Cryst. Res. Technol. 44 (11) (2009) 1230–1234.
[34] K.-T. Lee, N.-L. Wu, J. Power Sources 179 (2008) 430–434.
[35] C. Lin, J.A. Ritter, B.N. Popov, J. Electrochem. Soc. 145 (1998) 4097–4103.
[36] V. Srinivasan, J.W. Weidner, J. Power Sources 108 (2002) 15–20.
[37] E. Machefaux, T. Brousse, D. Bèlanger, D. Guyomard, J. Power Sources 165 (2007) 651–655.